




ORIGINAL ARTICLE

Relationship between time-to-isolation and freeze duration: Computational modeling of dosing for Arctic Front Advance and Arctic Front Advance Pro cryoballoons

Michael K. Getman MS¹  | Erik Wissner MD, PhD²  | Ravi Ranjan MD, PhD^{3,4,5}  | Jean-Pierre Lalonde BS⁶

¹Medtronic Inc, Minneapolis, Minnesota

²Division of Cardiology, University of Illinois Health, Chicago, Illinois

³Department of Medicine, Division of Cardiovascular Medicine, University of Utah, Salt Lake City, Utah

⁴Department of Biomedical Engineering, University of Utah, Salt Lake City, Utah

⁵Nora Eccles Harrison Cardiovascular Research and Training Institute, University of Utah, Salt Lake City, Utah

⁶Medtronic CryoCath, Pointe-Claire, Quebec, Canada

Correspondence

Michael K. Getman MS, Medtronic Inc, 8200 Coral Sea St NE, Mounds View, MN 55112.
Email: michael.k.getman@gmail.com

Disclosure: None.

Abstract

Background: Preclinical and clinical studies have utilized periprocedural parameters to optimize cryoballoon ablation dosing, including acute time-to-isolation (TTI) of the pulmonary vein, balloon rate of freezing, balloon nadir temperature, and balloon-thawing time. This study sought to predict the Arctic Front Advance (AFA) vs Arctic Front Advance Pro (AFA Pro) ablation durations required for transmural pulmonary vein isolation at varied tissue depths.

Methods: A cardiac-specific, three-dimensional computational model that incorporates structural characteristics, temperature-dependent cellular responses, and thermal-conductive properties was designed to predict the propagation of cold isotherms through tissue. The model assumed complete cryoballoon-to-pulmonary vein (PV) circumferential contact. Using known temperature thresholds of cardiac cellular electrical dormancy (at 23°C) and cellular nonviability (at -20°C), transmural time-to-isolation electrical dormancy (TTI_{ED}) and cellular nonviability (TTI_{NV}) were simulated. **Results:** For cardiac thickness of 0.5, 1.25, 2.0, 3.0, 4.0, and 5.0 mm, the 23°C isotherm passed transmurally in 33, 38, 46, 62, 80, and 95 seconds during cryoablation utilizing AFA and 33, 38, 46, 63, 80, and 95 seconds with AFA Pro. Using the same cardiac thicknesses, the -20°C isotherm passed transmurally in 40, 55, 78, 161, 354, and 696 seconds during cryoablation with AFA and 40, 54, 78, 160, 352, and 722 seconds with AFA Pro.

Conclusion: This model predicted a minimum duration of cryoballoon ablation (TTI_{NV}) to obtain a transmural lesion when acute TTI of the PV was observed (TTI_{ED}). Consequently, the model is a useful tool for characterizing CBA dosing, which may guide future cryoablation dosing strategies.

KEYWORDS

catheter ablation, computational modeling, cryoballoon, pulmonary vein isolation

Abbreviations: AF, atrial fibrillation; AFA, Arctic Front Advance, second-generation Medtronic cryoballoon; AFA Pro, Arctic Front Advance Pro, fourth-generation Medtronic cryoballoon; CBA, cryoballoon ablation; LA, left atrium; N₂O, nitrous oxide; PV, pulmonary vein; PVI, pulmonary vein isolation; TTI, time-to-isolation; TTI_{ED}, time-to-isolation electrical dormancy; TTI_{NV}, time-to-isolation nonviability.

This is an open access article under the terms of the Creative Commons Attribution-NonCommercial-NoDerivs License, which permits use and distribution in any medium, provided the original work is properly cited, the use is non-commercial and no modifications or adaptations are made.

© 2019 The Authors. *Journal of Cardiovascular Electrophysiology* Published by Wiley Periodicals, Inc.

1 | INTRODUCTION

The cryoballoon ablation (CBA) catheter has been used successfully to treat patients with atrial fibrillation (AF) by performing pulmonary vein isolation (PVI).¹⁻³ Traditional CBA-dosing protocols for the Arctic Front balloon (Medtronic, Inc) included multiple freeze applications with 240- to 360-second freeze durations, which were derived from preclinical animal testing, historic practices from focal cryogenic catheter usage, and typical user experience during the STOP-AF clinical trial (NCT00523978; Figure 1 and Table 1).^{19,20} Design improvements incorporated in the Arctic Front Advance (AFA; Medtronic, Inc) facilitated a more uniform cooling profile and enhanced energy transfer into the cardiac tissue.²¹ Initially, dosing conditions established for Arctic Front were transferred to AFA; however, the observed rates of adverse events and complications (eg, phrenic nerve injury, hemoptysis, and atrioesophageal fistula formation) with the AFA suggested that there was a deeper and/or faster cooling which potentially created a higher risk of collateral tissue damage when using historic dosing practices.^{10,11,22,23}

Consequently, studies were initiated to redefine AFA dosing parameters (Figure 1 and Table 1), including (a) examining the requirement for multiple cryofreeze applications (including the bonus freeze and freeze-thaw-refreeze applications); (b) evaluating reductions in freeze duration; and/or (c) investigating intraprocedural data with regard to balloon characteristics (eg, balloon nadir temperature, acute time-to-isolation [TTI], and balloon thaw time) that could be used to inform real-time, individualized dosing.^{15-18,24} Through these studies, TTI < 60 seconds has been identified as a strong intraprocedural predictor of CBA longer-term PVI durability.^{3,15-18,24} When observed, real-time TTI of pulmonary vein (PV) signals provide a measurable parameter of acute cardiac tissue damage that can predict a durable longer-term freedom from AF recurrence.^{15-18,24}

Recently, the Arctic Front Advance Pro (AFA Pro; Medtronic, Inc) has been used in limited commercial release.²⁵ The primary differentiation between AFA and AFA Pro is an approximately 40% reduction in the length of the distal nose of the AFA Pro which may improve the ability to achieve TTI recordings and enhance balloon catheter maneuverability within the left atrium (LA).²⁵ Importantly, with regard to ablation dosing, the internal balloon components and specifications remain unchanged between the AFA and AFA Pro.^{21,25} Based on catheter design similarities (ie, coolant flow rates and injection port locations), the a priori assumptions of transitive freeze characteristics were evaluated between both cryoballoon catheters to examine the similarities (or differences) of freeze parameter results. In our current modeling study of AFA and AFA Pro, we examined the temporal relationship between acute TTI and the minimum freeze duration by modeling lesion formation via the cold isotherms associated with cellular electrical dormancy (TTI_{ED}) and cellular nonviability (TTI_{NV}), respectively. Ultimately, these data may better inform future designs of dosing studies by minimizing energy transfer to collateral anatomical structures which may lead to a better optimized efficacy and safety profile when treating AF patients with AFA or AFA Pro.

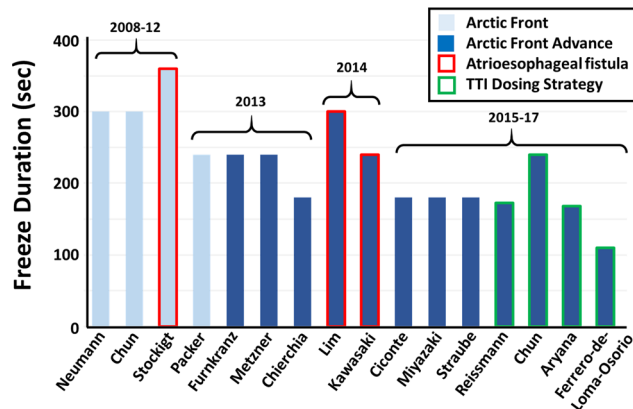


FIGURE 1 A reduction in freeze duration is observed after the reporting of atrioesophageal fistulas, after the introduction of the Arctic Front Advance cryoballoon, and after the implementation of time-to-isolation (TTI) studies

2 | METHODS

In our study, the three-dimensional computational model represents the ablation sequence of a typical cryoballoon application from the 28-mm AFA or AFA Pro. The clinical applications and methods of CBA have previously been well described.¹⁻³ In brief, the inflated balloon is

TABLE 1 Freeze duration and number of freeze applications reduced with further cryoballoon dosing studies

Reference	Freeze duration, s	Freeze number per PV
1. Neumann et al ⁴	300	3 freezes
2. Chun et al ⁵	300	2-5 freezes
3. Stöckigt et al ⁶	360	2-3 freezes
4. Packer et al ¹	240 (mean, 214)	3 freezes
5. Fürnkranz et al ⁷	240	2 freezes
6. Metzner et al ⁸	240	Single freeze
7. Chierchia et al ⁹	180	1.5 freeze
8. Lim et al ¹⁰	300	1-3 freezes
9. Kawasaki et al ¹¹	180-240	2-3 freezes
10. Ciconte et al ¹²	180	Single freeze
11. Miyazaki et al ¹³	180	Single freeze (except for LCPV)
12. Straube et al ¹⁴	180	3 freezes
13. Reissmann et al ¹⁵	TTI + 120 (~172)	Single freeze
14. Chun et al ¹⁶	240	Bonus freeze if TTI > 75 s
15. Aryana et al ¹⁷	TTI + 120 (~168)	Bonus freeze if TTI > 60 s
16. Ferrero-de-Loma-Osorio et al ¹⁸	TTI + 60 (~110)	Bonus freeze of 120 s

Abbreviations: LCPV, low-concentrating photovoltaic; PV, pulmonary vein; TTI, time-to-isolation.

positioned in the LA to engage the antral cardiac tissue surface of the PV. Liquid nitrous oxide (N_2O) is injected into the cryoballoon for a set duration. According to the Joule-Thomson effect, the N_2O phase change from liquid-to-gas consumes energy, and the resulting endothermic reaction creates a rapid decrease in temperature to a boiling point of -89.5°C at atmospheric pressure.²⁶ This endothermic process removes heat energy from cardiac tissue in contact with the distal hemisphere of the balloon surface, which results in the local creation of both intracellular and extracellular ice. The resulting biophysical process of cellular destruction concludes with a demarcated lesion or scar tissue and electrical isolation of the PV.^{2,3}

2.1 | Computational modeling

To computationally model this complex interaction of ice formation across cardiac tissue, we utilized the known physical constructs and thermodynamics. Specifically, the COMSOL Multiphysics software program (COMSOL v5.4; Burlington, MA) was used to simulate the heat transfer and blood flow behaviors in a nonisothermal flow module that took into account the physical constraints of cardiac anatomy near the PVs. Additionally, the time-dependent solver subfeature module was used to configure a fully coupled relationship of freeze dynamics across a tissue over a time-dependent calculation. These biological and physical assumptions were the core of the computational model and are further explained in detail by individual physiological interactions, including (a) physical interactions, (b) cellular heat loss, (c) tissue depth variables, and (d) the usage of different cryoballoons.

2.2 | Balloon-to-tissue interactions

The biophysical interactions of cold on cardiac tissue (ie, heat-energy loss) provides the foundational element for this model of lesion formation. Briefly, a circular 23-mm diameter PV with neutral angles towards the antral LA borders and uniform atrial tissue depths was generated for the model, which included neighboring tissue boundaries (Figure 2). The model assumed a balloon-to-PV circumferential contact zone that was minimally 2.0 mm in width, and the model also assumed that a 30g downward force was being applied during the balloon-to-PV occlusion and subsequent freeze application. Specifically, the 2.0-mm contact zone was a theoretical minimum contact patch when assuming that a circular 23-mm diameter PV comes into contact with a 28-mm cryoballoon in an axial orientation with a 30g pushing force. The contacting LA cardiac tissue (using Pennes' bioheat which include metabolic heat generation and perfusion) and circulating blood flow (from the PV and LA chamber) both act as heat sources while the cryoballoon becomes the heat sink during the balloon ablation. Tissue temperature dynamics associated with Pennes' bioheat are incorporated and appropriately scaled (while the tissue is in a nonfrozen temperature range). Similarly, the PV blood circulation is appropriately scaled as a heat source while in a nonfrozen state during the balloon-to-PV occlusion. With regard to LA blood circulation, the thermal modeling assumes a 12-cm/s blood flow within the LA chamber, in accordance with measurements within

AF patients in sinus rhythm.^{27,28} In brief summary of this computational model, the fundamental assumed parameters are the idealized balloon-to-tissue interfacing boundaries and the thermodynamic heat (source and sink) exchanges, which then predict a progression of cold through the cardiac tissue and a resulting cellular response (and subsequent lesion formation in the manner of a PVI).

2.3 | Cellular response to heat-energy loss

As N_2O undergoes a liquid-to-gas phase shift (under Joule-Thomson conditions within the cryoballoon); heat from the surrounding cardiac tissue is withdrawn, and a cold isotherm propagates outward from the balloon-to-tissue interface as a function over time.²⁶ Specifically, our model focuses on two isothermal processes that have been determined to elicit a cellular response, which are later indicative of critical steps in the lesion formation after CBA. The first critical isotherm (23°C) represents the point at which myocardial cells exhibit a significant decline and ultimate cessation of electrophysiological activity (ie, electrical dormancy; TTI_{ED}).²⁹⁻³¹ For this study, it was modeled that when this isotherm achieved circumferential transmurally the electrical PV potentials became acutely isolated, which was denoted as the time-to-isolation for electrical dormancy (TTI_{ED}). TTI_{ED} in this model represented acute TTI which is typically observed in the clinical electrophysiology laboratory during cryoballoon ablation of a PV. More specifically, it is the point at which PV electrical potentials become disassociated with the LA chamber during cryoablation. The second critical isotherm during a cryoablation (-20°C) represents the point at which myocardial cells reach nonviability.^{32,33} In our current modeling study, the time-to-isolation for nonviability (TTI_{NV}) was denoted and modeled as the critical point whereby the isotherm achieves a circumferentially transmural temperature of -20°C and the cells become irreversibly nonviable. TTI_{NV} in this model represented the minimum freeze duration required for permanent cellular damage. Ultimately, the computer model will determine the spatial range of cold propagation during

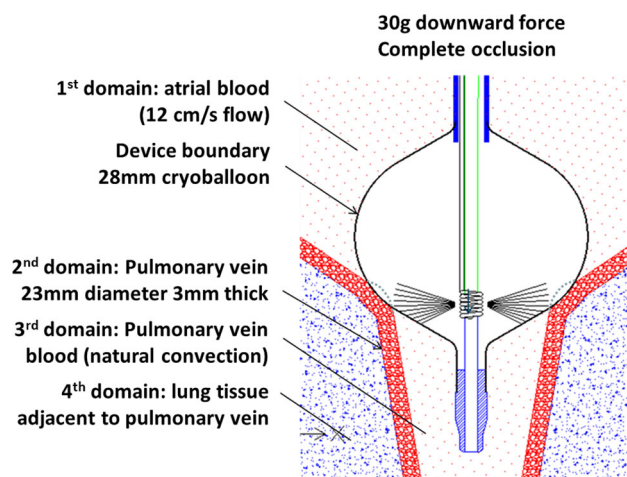


FIGURE 2 Schematic representation of the thermal boundary conditions and primary domains

TTI_{ED} and TTI_{NV} (Figure 3). Further, the model will derive a response formula between TTI_{ED} and TTI_{NV} timing of events across different cardiac tissue thicknesses (Figure 4).

2.4 | Tissue depth

The distribution of temperature decay is not uniform from the cryoballoon surface onto the contacted cardiac tissue.³⁴ Specifically, the isotherm propagates into the cardiac tissue maximally at the center-point of balloon-to-tissue contact, and the coldest temperatures within the cryoballoon (AFA or AFA Pro) are obtained at the eight points of N_2O phase shift (whereby the liquid spray of N_2O from eight separate ports contacts the inner balloon surface). Consequently, it was critical to conduct computational modeling simulations with varying degrees of cardiac tissue depth to account for the engineered balloon variability (eg, balloon size and catheter models) and the human cardiac anatomy variability.³⁵

Regarding LA and PV anatomies, a previous imaging study determined that the LA wall thickness in patients undergoing PVI had an average thickness of 1.89 ± 0.48 mm (range, 0.5–3.5 mm).³⁵ This information drove the primary assumed variable within the model, which was LA tissue thickness near the PV. In our model, simulations were performed with tissue depths of 0.5, 1.25, 2.0, 3.0, 4.0, and 5.0 mm. A convergence study was conducted for each tissue depth to verify the results were independent of the mesh size. These set distances of transmural cold propagation into the cardiac tissue allowed for the assessment of decreasing temperature distribution with regard to TTI_{NV} and the evaluation of cold transfer into collateral tissue. By adjusting the cardiac thickness values within the computational model, the simulations determined the cryoablation freeze durations required for the circumferential and transmural delivery of the electrical dormancy and nonviability isotherms.

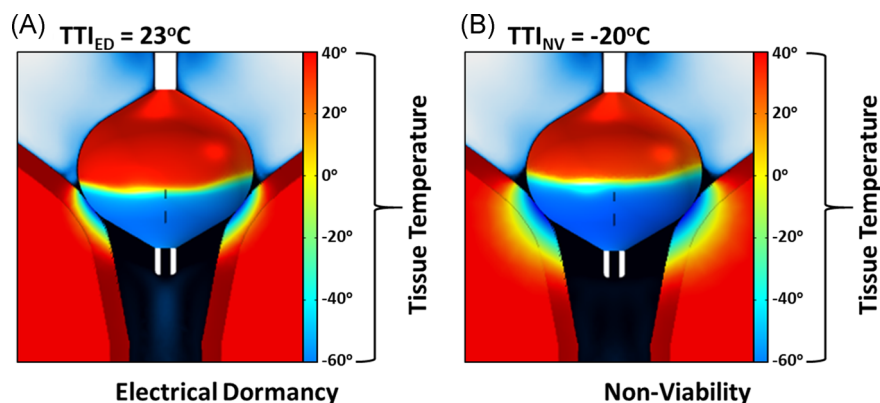


FIGURE 3 Illustration of the modeled cold propagation into 3-mm depth cardiac tissue at different temperatures. The dark red is a visual representation of the pulmonary vein boundary and the light red is a visual representation of adjacent non-PV tissue. A, Electrical dormancy isotherm (23°C) is circumferentially transmural. B, Thermal profile at -20°C , which is the temperature achieved at cellular nonviability. PV, pulmonary vein; TTI_{ED} , time-to-isolation electrical dormancy; TTI_{NV} , time-to-isolation nonviability

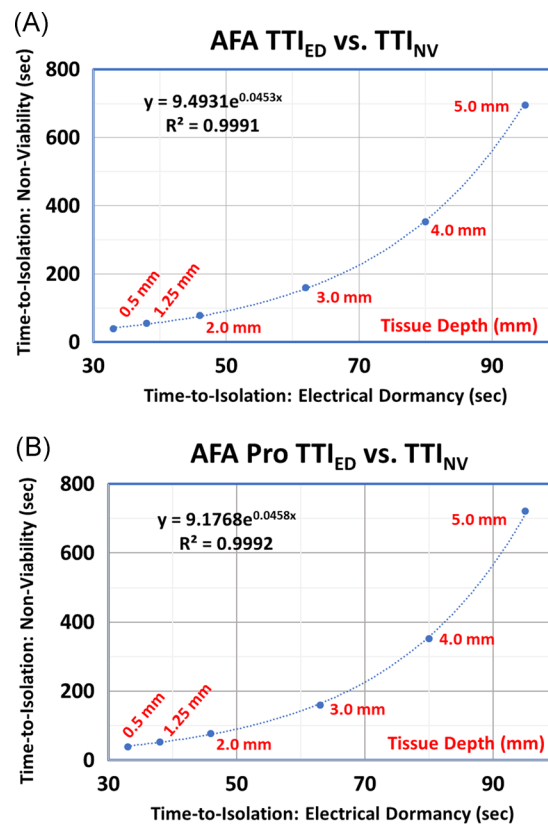


FIGURE 4 A, The relationship between the time to achieve cellular electrical dormancy (TTI_{ED}) and the time to achieve cellular nonviability (TTI_{NV}) with Arctic Front Advance at discrete tissue depths. B, The relationship between the time to achieve cellular electrical dormancy (TTI_{ED}) and the time to achieve cellular nonviability (TTI_{NV}) with Arctic Front Advance Pro at discrete tissue depths. AFA, Arctic Front Advance; AFA Pro, Arctic Front Advance Pro; TTI_{ED} , time-to-isolation electrical dormancy; TTI_{NV} , time-to-isolation nonviability

2.5 | AFA vs AFA Pro

The similarly designed 28-mm AFA and AFA Pro were incorporated into the model to confirm the assumptions of transitive clinical effect. Simply, the AFA Pro catheter was built on the AFA platform, with the same internal balloon components and specifications.²⁵ The primary difference between the two cryoballoon catheters is a 40% reduction in distal-tip length from AFA to AFA Pro (13.5 vs 8 mm). This change in AFA Pro was designed to increase maneuverability within the LA and increase the probability of recording PV potentials with the Achieve Inner-lumen Mapping Catheter (Medtronic, Inc).²⁵ Consistent between both balloons, the injection tube coil remains 21.5-mm distal to the thermal-couple location, and thus, the N₂O spray pattern and return gas temperature recordings are unchanged between AFA and AFA Pro.²⁵ Most importantly, there is little expected thermodynamic change that is “a priori” predicted between the two balloon catheters; however, the purpose of utilizing the two cryoballoon systems was to test the importance of homogeneity within the balloon internal specifications vs discrete changes to the external balloon components.

3 | RESULTS

Our computational model tracks change in temperature over time and distance. With the known temperature changes through tissue depths during cryoablation, the output solves for the time required for the TTI_{ED} and TTI_{NV} isotherms to reach full circumferential transmural for the defined tissue depth(s).

3.1 | Establishment of the computational model

To examine the computational model accuracy, the mesh convergence study performed for each of the tissue depths resulted in a variance of ±8% to ensure the results were independent of mesh size. The cylindrical model dimensions were identified to be sufficiently large as to not influence the results. Figure 3 depicts AFA Pro's thermal profile of the 3-mm tissue depth construct when TTI_{ED} was reached in 63 seconds (Panel A) and TTI_{NV} reached in 160 seconds (Panel B). The cold propagation was observed from the surface of the balloon as the freeze duration progressed until a temperature of electrical dormancy was achieved (orange-colored isotherm). As the freeze continues, the isotherm associated with electrical dormancy continued to progress deeper into the cardiac tissue (Supporting Information Video S1). Of note, in our computational model, the progression of the cold isotherms effect the blood pool that was in contact with the balloon (as well as the tissue that is in direct contact). In our model, the ice cap within the pulmonary vein forms within 35 seconds and will continue to grow at a decaying speed.

3.2 | Relationship between TTI_{ED} and TTI_{NV}

Tables 2 and 3 display the TTI_{ED} and TTI_{NV} for each simulation performed for the AFA and AFA Pro catheters at tissue depths of 0.5,

TABLE 2 Elapsed time to achieve TTI_{ED} and TTI_{NV} across several cardiac tissue depths for Arctic Front Advance

Tissue depth, mm	TTI _{ED} , s	TTI _{NV} , s
0.5	33	40
1.25	38	55
2.0	46	78
3.0	62	161
4.0	80	354
5.0	95	696

Abbreviations: TTI_{ED}, time-to-isolation electrical dormancy; TTI_{NV}, time-to-isolation nonviability.

1.25, 2.0, 3.0, 4.0, and 5.0 mm. For the AFA balloon, TTI_{ED} was established at 33, 38, 46, 62, 80, and 95 seconds, respectively. By comparison, the AFA Pro established TTI_{ED} at 33, 38, 46, 63, 80, and 95 seconds, respectively. The influence of the shortened distal nose tip on the AFA Pro was minimal as both balloon catheters demonstrated similar TTI_{ED} across the different tissue depths. When examining TTI_{NV}, the AFA balloon was able to establish this isotherm progression at 40, 55, 78, 161, 354, and 696 seconds, respectively. For comparison, the AFA Pro demonstrated TTI_{NV} at 40, 54, 78, 160, 352, and 722 seconds, respectively. Again, the AFA and AFA Pro were similar with regard to TTI_{NV} with no more than 4% variance at 5.0 mm between the two balloons when establishing cellular nonviability.

As the tissue depth increases beyond 2.0 mm in the computational model, the time separating TTI_{ED} and TTI_{NV} expanded. Figure 4A and 4B illustrate a positive nonlinear relationship between TTI_{ED} and TTI_{NV} with progressing tissue thickness. The line of best-fit identifies the equation to be nonlinear ($TTI_{NV} = 9.4931e^{0.0453 \times TTI_{ED}}$; $R^2 = 0.9991$) for AFA. Similarly, line of best-fit for AFA Pro identifies the equation to be nonlinear ($TTI_{NV} = 9.1768e^{0.0458 \times TTI_{ED}}$; $R^2 = 0.9992$). Both equations between balloons were remarkably similar and demonstrate the positive but nonlinear response as the cardiac tissue becomes thicker in depth, suggesting that there is a physical limit to cold propagation given the current cryoballoon design parameters (eight injection ports, N₂O spray rate, refrigerant characteristics, etc).

TABLE 3 Elapsed time to achieve TTI_{ED} and TTI_{NV} across several cardiac tissue depths for Arctic Front Advance Pro

Tissue depth (mm)	TTI _{ED} , s	TTI _{NV} , s
0.5	33	40
1.25	38	54
2.0	46	78
3.0	63	160
4.0	80	352
5.0	95	722

Abbreviations: TTI_{ED}, time-to-isolation electrical dormancy; TTI_{NV}, time-to-isolation nonviability.

4 | DISCUSSION

This current study models the thermal propagation of cold through tissue using manufacturer knowledge of the heat-energy transfer function between the cryoballoon and contacting antral LA cardiac surface. Specifically, the study models the lesion formation based on a cardiac tissue response to the thermodynamic changes of the freeze application within the cryoballoon catheter. The data from this computational model illustrates the positive nonlinear relationship between TTI_{ED} and TTI_{NV} through different measured cardiac tissue depths (Figures 3 and 4). The data confirms that AFA and AFA Pro shared similar thermodynamic characteristics, as the internal components remained unchanged between the two balloon catheters.²⁵ The results of this computational modeling were functional formulas (specifically for AFA and AFA Pro; Figures 3 and 4) that describes the positive nonlinear relationship between the cellular electrical dormancy and cellular nonviability (AFA: $TTI_{NV} = 9.4931e^{0.0453 \times TTI_{ED}}$; $R^2 = 0.9991$ and AFA Pro: $TTI_{NV} = 9.1768e^{0.0458 \times TTI_{ED}}$; $R^2 = 0.9992$) during a freeze application. The modeled transfer-functions of cold propagation agreed with the learned clinical practice(s) that had evolved through the historic usage of the AFA ablation catheter.²⁴ Specifically, when TTI_{ED} was obtained in under 60 seconds, physician users have developed algorithms that continued the freeze application for a total ablation time of about 180 seconds.^{15,24} More importantly, these shortened single-freeze dosing strategies using TTI_{ED} were found to have robust longer-term efficacy in prospective studies.²⁴ Last, there has not been a large randomized controlled clinical study to establish a set dosing standard, and the larger variety of user habits may make such a study impossible and/or impractical (eg, differences in patient selection, preprocedural imaging, sedation, over-the-wire delivery, occlusion testing, anatomical ablation strategy, freeze termination rules, etc). Consequently, the important work done in computer modeling, animal studies, clinical trials, and real-world clinical dosing algorithms are the only avenues to set-up common and/or well-practiced dosing guidance.^{1,2,15,18,21,24}

4.1 | Previous modeling and experiments

Similar in vivo experiments have been conducted that measure the cryoballoon freeze characteristics under different study design parameters.^{36,37} Specifically, direct surgical attachment of thermocouples into cardiac and surrounding tissues in canine models have measured time, temperature, and distance relationships during a cryoballoon freeze.^{36,37} In general, our computational modeling data agree with these data, albeit with small differences (warmer temperatures in the canine models) with regard to the nadir temperature ranges observed within cardiac and surrounding tissues.^{36,37} These discrepancies between our model and the previous canine studies may be the result of one or several factors, including (a) computational modeling over simplifies real-world observations (with a limitation on the number of inputting variables); (b) open-chest testing done in an in vivo model may influence

temperature recording (as the ambient air environment acts as an erroneous heat sink); and/or (c) the precision and accuracy of recorded in vivo parameters (compared to the computational modeling) may have inherent real-world deviations because of “true” experimental variability (eg, intraprocedural and interprocedural changing cardiac tissue thickness and/or heterogeneity in tissue composition). However, having directionally concordant data between our computational modeling and the in vivo experiment bolsters the understanding of the basic thermodynamic principles. Specifically, it demonstrates the positive nonlinear relationships of cold temperature propagation over a distance through cardiac tissue (with regard to TTI_{ED} and TTI_{NV}). Last, it must be acknowledged that a previous attempt to model the thermodynamic properties of the cryoballoon has been reported.³⁸ However, without direct knowledge of the proprietary cryoballoon specifications, this previous study (from an independent research group) was limited in the predictive power of the computational model.

4.2 | Real-world usage of time-to-isolation

In clinical practice and study design, TTI (aka, time-to-effect) has been used to denote TTI_{ED} , and the additional freeze duration (time beyond TTI_{ED}) has allowed for additional temperature decline within the targeted cardiac-ablation zone until TTI_{NV} is achieved.^{15,24} In our computational model, TTI_{ED} was achieved in about 60 seconds when the cardiac tissue was 3 mm at the targeted site of ablation. Furthermore, TTI_{NV} was obtained within 180 seconds when the freeze duration was extended at this hypothetical depth of ablation. For cardiac tissue thicknesses of 0.5 through 3 mm the response interaction was mostly linear (Figures 3 and 4); however, at tissue depths of 4 and 5 mm, the additional freeze time to achieve TTI_{NV} was prolonged. Our exponential freeze-response curve is similar to the real-time cryoablation measurements recorded using magnetic resonance imaging (MRI).³⁹ Specifically, a study by Lichter et al³⁹ determined by MRI that the normalized area of freeze increased rapidly from the start of cryoablation through 120 seconds, and a further increase in area of freeze was observed at 180 seconds (although the latter had a diminished rate of freeze area increase). Last, very little continued growth of the freeze area was observed between 180 and 240 seconds by MRI measurements.³⁹ This very slow rate of increase beyond the initial 120 seconds explains the very prolonged TTI_{NV} at higher depths.

Not surprisingly, empirical clinical dosing has arrived at a similar dosing paradigm well before our modeled computations. Specifically, it is common to ablate a PV for an overall duration of 180 seconds when TTI_{ED} is less than 60 seconds.³ Our model determined TTI_{ED} could be achieved in 63 seconds and TTI_{NV} in 160 seconds when the cardiac tissue was 3-mm thick. Furthermore, several clinical cryoballoon dosing algorithms have based the success parameter of acute PVI on the ability to obtain TTI within and around 60 seconds.^{15-18,24} More specifically, the usage of TTI+120 seconds is a strategy used in previous studies that have evaluated dosing algorithms and longer-term PVI durability.^{3,15,24} Given that our computational values are true (at a “normal” cardiac tissue depth of about 3 mm); a “good” freeze

attempt with the cryoballoon should achieve TTI_{ED} within approximately 60 seconds (when PV potentials are viewable). When TTI_{ED} is not achieved in 60 seconds, an abort of the freeze and repositioning of the cryoballoon may be a better dosing strategy.²⁴ However, these aforementioned dosing algorithms must consider cardiac tissue depths at known anatomical structures.³¹ As an example, it would be expected that TTI_{ED} is extended when the cryoballoon is ablating along a thickened cardiac anatomy such as the ridge between PV and left atrial appendage. Ultimately, our computational model data might further progress dosing strategies and algorithms that continue to attempt to shorten the cryoablation freeze duration.⁴⁰

4.3 | The future of computational model data usage

Our current study precisely examined only the relationship between TTI across two separate cryoballoons; however, the computational model foundation that was established in this study can be expanded into future uses. For instance, if a larger diameter cryoballoon is developed, the predicted characteristics of the current balloon isotherm propagation would then be used to characterize and inform the design of the N_2O spray performance that would maintain similar balloon cooling characteristics. Additionally, several “newer” balloons are being developed to enter into commercial markets. Computational modeling with those balloons may provide initial insight into whether traditional parameters used to predict outcomes with the Arctic Front family of cryoballoons can be transferred to the newer balloon technologies or if balloon-specific parameters need to be developed for new catheter ablation technologies. Ultimately, with newer balloons coming into commercial markets, a better “predicted” route of safe and effective dosing would be greatly appreciated.

This model establishes the foundational parameters and behaviors of the AFA and AFA Pro in an idealized coaxial occlusion state. The data presented is consistent with clinical dosing studies employed today. Continuation of this study will explore real-world input factors that may influence the distribution of isotherms through tissue. Further model development will continue to consider more real-world usages and habits, including (a) modeling more extensively the anatomical variations (ie, vein shape/dimensions, heterogenous tissue depths, tissue scar, common ostia, and discrete collateral tissue (eg, phrenic nerve)); (b) modeling more periprocedural interactions (ie, catheter orientation, variable balloon-tissue contact zones, and multiple refreezes); and (c) modeling different periprocedural technical usages (ie, balloon pull-down technique and nonocclusive ablation). Ultimately, it is expected that these next series of computer models will enhance our understanding of AFA and AFA Pro under different usage conditions.

5 | LIMITATIONS

The validity of computational modeling is foundational to the assumed variables and parameters that were captured in the mathematical inputs. In our model, the PV was perfectly circular

with consistent (and discrete) depths of tissues having homogeneous tissue characteristics and idealized coaxial cryoballoon positioning, assuming perfect occlusion. While these assumptions were “built-in” to manage the complexity of the model; it is recognized that there is variability and heterogeneity in the previous real-world parameters. Further, our computational model assumes a decay input to Pennes’ bioheat equation between 37°C and 23°C, the temperature at which no heat is generated by tissue. Similarly, localized vascular perfusion was assumed to slow between 37°C and become negligible at 0°C. For all the above modeling characteristics, this computational model may be simplified, and yet, the direct data finding from this model are remarkably similar to the empirical clinical cryoballoon dosing habits and real-time MRI recordings.

The modeling was performed with AFA and AFA Pro. These are the second-generation and fourth-generation cryoballoons. The third-generation (Arctic Front Advance ST) has been removed from distribution due to manufacturability. There were significant design changes from AFA to AFA ST that would present differences in the cold transfer and temperatures captured. These design changes were identified and corrected when AFA Pro was created.

Last, our computational modeling was limited to clinically relevant cardiac tissue depths and clinically relevant usage conditions of the cryoballoon. Of note, we did not model tissue depths to 10 mm, and we did not consider the extended cryoballoon freeze duration to achieve a 10-mm freeze depth. While a theoretical computational model can calculate the above parameters, we made every attempt to restrain modeling assumptions and usage conditions to clinically relevant real-world usage parameters.


6 | CONCLUSION

The computational model predicts a minimum duration of freeze (TTI_{NV}) needed to obtain a durable and transmural lesion when acute TTI of the PV is observed (TTI_{ED}). This can be used clinically to titrate CBA rather than using empiric freeze times-minimizing procedure durations and potentially reduce collateral tissue damage. The computational model of CBA can be further used for future clinical investigations to optimize CBA for different anatomies or targeting beyond the PV anatomy.

CONFLICT OF INTERESTS

Michael K. Getman and Jean-Pierre Lalonde are employees of Medtronic. Dr. Wissner has received consulting fees, speaker’s honoraria, and educational fellowship funding from Medtronic. Dr. Ranjan is supported by NIH grant R01 HL142913 and has research grants from Abbott and is a consultant to Medtronic and Abbott.

ORCID

Michael K. Getman  <http://orcid.org/0000-0002-2850-3756>
Erik Wissner  <http://orcid.org/0000-0002-7033-567X>
Ravi Ranjan  <http://orcid.org/0000-0002-3321-2435>

REFERENCES

- Packer DL, Kowal RC, Wheelan KR, et al. Cryoballoon ablation of pulmonary veins for paroxysmal atrial fibrillation. *J Am Coll Cardiol*. 2013;61(16):1713-1723.
- Su W, Kowal R, Kowalski M, et al. Best practice guide for cryoballoon ablation in atrial fibrillation: the compilation experience of more than 3000 procedures. *Heart Rhythm*. 2015;12(7):1658-1666.
- Su W, Aryana A, Passman R, et al. Cryoballoon best practices II: practical guide to procedural monitoring and dosing during atrial fibrillation ablation from the perspective of experienced users. *Heart Rhythm*. 2018;15(9):1348-1355.
- Neumann T, Vogt J, Schumacher B, et al. Circumferential pulmonary vein isolation with the cryoballoon technique. *J Am Coll Cardiol*. 2008;52(4):273-278.
- Chun KRJ, Schmidt B, Metzner A, et al. The 'single big cryoballoon' technique for acute pulmonary vein isolation in patients with paroxysmal atrial fibrillation: a prospective observational single centre study. *Eur Heart J*. 2009;30(6):699-709.
- Stöckigt F, Schrickel JW, Andrié R, Lickfett L. Atrioesophageal fistula after cryoballoon pulmonary vein isolation. *J Cardiovasc Electrophysiol*. 2012;23:1254-1257.
- Fürnkranz A, Bordignon S, Schmidt B, et al. Improved procedural efficacy of pulmonary vein isolation using the novel second-generation cryoballoon. *J Cardiovasc Electrophysiol*. 2013;24:492-497.
- Metzner A, Burchard A, Wohlmuth P, et al. Increased incidence of esophageal thermal lesions using the second-generation 28-mm cryoballoon. *Circ Arrhythm Electrophysiol*. 2013;6:769-775.
- Chierchia GB, Di Giovanni G, Sieira-Moret J, et al. Initial experience of three-minute freeze cycles using the second-generation cryoballoon ablation: acute and short-term procedural outcomes. *J Interv Card Electrophysiol*. 2013;39:145-151.
- Lim HW, Cogert GA, Cameron CS, Cheng VY, Sandler DA. Atrioesophageal fistula during cryoballoon ablation for atrial fibrillation. *J Cardiovasc Electrophysiol*. 2014;25(2):208-213.
- Kawasaki R, Gauri A, Elmouchi D, Duggal M, Bhan A. Atrioesophageal fistula complicating cryoballoon pulmonary vein isolation for paroxysmal atrial fibrillation. *J Cardiovasc Electrophysiol*. 2014;25(7):787-792.
- Ciconte G, de Asmundis C, Sieira J, et al. Single 3-minute freeze for second-generation cryoballoon ablation: one-year follow-up after pulmonary vein isolation. *Heart Rhythm*. 2015;12:673-680.
- Miyazaki S, Hachiya H, Nakamura H, et al. Pulmonary vein isolation using a second-generation cryoballoon in patients with paroxysmal atrial fibrillation: one-year outcome using a single big-balloon 3-minute freeze technique. *J Cardiovasc Electrophysiol*. 2016;27:1375-1380.
- Straube F, Dorwarth U, Hartl S, et al. Outcome of paroxysmal atrial fibrillation ablation with the cryoballoon using two different application times: the 4- versus 3-min protocol. *J Interv Card Electrophysiol*. 2016;45:169-177.
- Reissmann B, Wissner E, Deiss S, et al. First insights into cryoballoon-based pulmonary vein isolation taking the individual time-to-isolation into account. *Europace*. 2017;19(10):1676-1680.
- Chun KRJ, Stich M, Fürnkranz A, et al. Individualized cryoballoon energy pulmonary vein isolation guided by real-time pulmonary vein recordings, the randomized ICE-T trial. *Heart Rhythm*. 2017;14(4):495-500.
- Aryana A, Mugnai G, Singh SM, et al. Procedural and biophysical indicators of durable pulmonary vein isolation during cryoballoon ablation of atrial fibrillation. *Heart Rhythm*. 2016;13(2):424-432.
- Ferrero-de-Loma-Osorio Á, García-Fernández A, Castillo-Castillo J, et al. Time-to-effect-based dosing strategy for cryoballoon ablation in patients with paroxysmal atrial fibrillation: results of the plusONE Multicenter Randomized Controlled Noninferiority Trial. *Circ Arrhythm Electrophysiol*. 2017;10(12):e005318. <https://doi.org/10.1161/CIRCEP.117.005318>
- van Belle Y, Janse P, Rivero-Ayerza MJ, et al. Pulmonary vein isolation using an occluding cryoballoon for circumferential ablation: feasibility, complications, and short-term outcome. *Eur Heart J*. 2007;28(18):2231-2237.
- Klein G, Oswald H, Gardiwal A, et al. Efficacy of pulmonary vein isolation by cryoballoon ablation in patients with paroxysmal atrial fibrillation. *Heart Rhythm*. 2008;5(6):802-806.
- Coulombe N, Paulin J, Su W. Improved in vivo performance of second-generation cryoballoon for pulmonary vein isolation. *J Cardiovasc Electrophysiol*. 2013;24(8):919-925.
- Mugnai G, de Asmundis C, Velagic V, et al. Phrenic nerve injury during ablation with the second-generation cryoballoon: analysis of the temperature drop behaviour in a large cohort of patients. *Europace*. 2016;18(5):702-709.
- Verma N, Gillespie CT, Argento AC, et al. Bronchial effects of cryoballoon ablation for atrial fibrillation. *Heart Rhythm*. 2017;14(1):12-16.
- Aryana A, Kenigsberg DN, Kowalski M, et al. Verification of a novel atrial fibrillation cryoablation dosing algorithm guided by time-to-pulmonary vein isolation: results from the Cryo-DOSING Study (Cryoballoon-ablation DOSING based on the assessment of time-to-effect and pulmonary vein isolation guidance). *Heart Rhythm*. 2017;14(9):1319-1325.
- Moltrasio M, Tundo F, Fassini G, Sicuso R, Cellucci S, Tondo C. Cryoablation of atrial fibrillation with the fourth-generation balloon: The first reported case. *Pacing Clin Electrophysiol*. 2019;42:553-556. <https://doi.org/10.1111/pace.13562>
- Gage AA, Baust J. Mechanisms of tissue injury in cryosurgery. *Cryobiology*. 1998;37(3):171-186.
- Markl M, Lee DC, Ng J, Carr M, Carr J, Goldberger JJ. Left atrial 4-dimensional flow magnetic resonance imaging: stasis and velocity mapping in patients with atrial fibrillation. *Invest Radiol*. 2016;51(3):147-154.
- Lee DC, Markl M, Ng J, et al. Three-dimensional left atrial blood flow characteristics in patients with atrial fibrillation assessed by 4D flow CMR. *Eur Heart J Cardiovasc Imaging*. 2016;17(11):1259-1268.
- Aufderheide T. Etiology, electrophysiology, and myocardial mechanics of pulseless electrical activity. *Cardiac Arrest, The Science and Practice of Resuscitation Medicine*. 2nd ed. New York: Cambridge University Press; 2007.
- Woodhall B, Sealy WC, Hall KD, Floyd WL. Craniotomy under conditions of quinidine-protected cardioplegia and profound hypothermia. *Ann Surg*. 1960;152:37-44.
- Khaladj N, Shrestha M, Meck S, et al. Hypothermic circulatory arrest with selective antegrade cerebral perfusion in ascending aortic and aortic arch surgery: a risk factor analysis for adverse outcome in 501 patients. *J Thorac Cardiovasc Surg*. 2008;135(4):908-914.
- Choi J, Bischof JC. Thermal thresholds of cardiovascular HL-1 cell destruction by cryothermal exposure. *Cryobiology*. 2017;78:115-118.
- Choi J, Bischof JC. Cooling rate dependent biophysical and viability response shift with attachment state in human dermal fibroblast cells. *Cryobiology*. 2011;63(3):285-291.
- Ciconte G, Coulombe N, Brugada P, de Asmundis C, Chierchia GB. Towards a tailored cryo-pulmonary vein isolation. Lessons learned from second-generation cryoballoon ablation. *Trends Cardiovasc Med*. 2019;29:420-425. <https://doi.org/10.1016/j.tcm.2018.11.009>
- Beinart R, Abbara S, Blum A, et al. Left atrial wall thickness variability measured by CT scans in patients undergoing pulmonary vein isolation. *J Cardiovasc Electrophysiol*. 2011;22(11):1232-1236.
- Takami M, Misiri J, Lehmann HI, et al. Spatial and time-course thermodynamics during pulmonary vein isolation using the second-generation cryoballoon in a canine in vivo model. *Circ Arrhythm Electrophysiol*. 2015;8(1):186-192.

37. Takami M, Lehmann HI, Misiri J, et al. Impact of freezing time and balloon size on the thermodynamics and isolation efficacy during pulmonary vein isolation using the second generation cryoballoon. *Circ Arrhythm Electrophysiol*. 2015;8(4):836-845.
38. Müssig R, Müssig R, Hörth J. Cryoballoon model and simulation of catheter ablation for pulmonary vein isolation in atrial fibrillation. *Curr Direct Biomed Eng*. 2018;4(1):473-475.
39. Lichter J, Kholmovski EG, Coulombe N, et al. Real-time magnetic resonance imaging-guided cryoablation of the pulmonary veins with acute freeze-zone and chronic lesion assessment. *Europace*. 2019;21(1):154-162.
40. Molenaar MMD, Timmermans CC, Hesselink T, et al. Shorter cryoballoon applications times do effect efficacy but result in less phrenic nerve injury: Results of the randomized 123 study. *Pacing Clin Electrophysiol*. 2019;42:508-514. <https://doi.org/10.1111/pace.13626>

SUPPORTING INFORMATION

Additional supporting information may be found online in the Supporting Information section.

How to cite this article: Getman MK, Wissner E, Ranjan R, Lalonde J-P. Relationship between time-to-isolation and freeze duration: Computational modeling of dosing for Arctic Front Advance and Arctic Front Advance Pro cryoballoons. *J Cardiovasc Electrophysiol*. 2019;30:2274-2282. <https://doi.org/10.1111/jce.14150>